# Electro-mechanical interactions in a DFIG drivetrain

Inaki Erazo-Damian *, Matteo F. Iacchetti, Judith M. Apsley

Power and Energy division, University Of Manchester, Sackville Street building M13 9PL, Manchester, UK
*inaki.erazodamian@manchester.ac.uk

**Abstract: Normally, electrical and mechanical systems are designed and analysed in separate domains but, in this paper, interactions between electric and mechanical elements are analysed looking for improvement in the performance of electro-mechanical drivetrains. The work considers a Doubly Fed Induction Generator (DFIG), evaluated with a frequency analysis of the full electro-mechanical drivetrain developed and applied to identify how tuning gains and system parameters affect the electro-mechanical interactions. Analytical transfer functions are presented and validated by simulation and test results.**

## Nomenclature

| | |
|---|---|
| **C** | Damping matrix |
| $i_s$, $i_r$ | Stator, rotor current |
| **K** | Stiffness matrix |
| *kp*, *ki*, *kf* | Proportional, integral and forward gains |
| $L_m$, $L_r$, $L_s$, $L_l$ | Mutual, rotor, stator, leakage inductance |
| **M** | Mass matrix |
| *pp* | Pole pairs |
| **q** | Mechanical state (output) vector |
| **Q** | Mechanical forcing term (input) vector |
| *R* | Resistance |
| $T_G$ | *DFIG* electromagnetic torque |
| $t_s$ | Switching period |
| $v_s$, $v_r$ | Stator, rotor voltage |
| $\theta_G$ , $\theta_r$ | Rotor mechanical, electrical angle ($\theta_r = pp\theta_G$) |
| $\theta_s^*$, $\theta_{slip}$ | Stator reference, slip electrical angle |
| $\psi_s$, $\psi_r$ | Stator, rotor flux linkage |
| $\omega_f$ | Filter cutoff frequency |
| $\omega_n$ | Mechanical natural frequency |
| $\omega_r$, $\omega_s$ | Rotor electrical speed, stator frequency |

## Superscript/subscript

| | |
|---|---|
| * | Set point |
| $\bar{A}$ | Complex quantity |
| *s*, *r* | Stator, rotor |
| *DC*, *G*, *Fly* | DC motor, DFIG, Fly-wheel parameters |
| *GBX*, *T* | Gearbox, Turbine parameters |
| *d*, *q* | Stator-flux oriented frame |
| *v*, *i* | Voltage and current controller |
| 0 | Steady state value |

## 1. Introduction

In many generation systems, the electrical generator is connected to the mechanical prime mover through a series of shafts, couplings and gear stages, in order to make the generator more accessible, or to change the speed ratio between the prime mover and the electrical network. The mechanical drivetrain possesses natural resonant modes, which if excited can give rise to excessive vibrations, causing wear and damage to components [1]. This has become a design consideration in multiple sectors such as wind energy conversion, transport on-board generation or propulsion and industrial drives, where increasing power density requirements make drivetrains more exposed to develop unwanted interactions between mechanical and control modes [2]. In stand-alone systems in particular the presence of highly dynamic loads can create torque perturbations potentially exciting drivetrain resonances. Broadly speaking, this issue is not confined to stand-alone generation systems for renewables but concerns vehicle applications as well and has led to a re-evaluation of options for electric power systems, electric propulsion, engine starter/generators, auxiliary power units, environmental control systems and electromechanical actuators [3]-[4].

Analysis of electromechanical interactions between generator, grid and drive-train has been carried out for grid-connected Doubly-Fed Induction Generators (DFIGs) and PM generators in wind energy conversion systems (WECS) [5]-[6], for up to a three-inertia model. Wind Turbine (WT) simulation tools [6]-[7] investigate the effects of the interaction of both domains using different generators.

A DFIG offers advantages of a fully controllable frequency and voltage output with a variable rotor speed of around ±30% with respect to the synchronous speed, while using a partially-rated converter. DFIGs have been extensively applied to wind power generation: Many control and connection schemes have been developed looking at grid-connected and stand-alone systems under balanced and unbalanced conditions, sensor-less control and giving operation, control and design principles for the different configurations [9]. Field-oriented control along the stator flux is adopted as a standard control technique for DFIGs in grid-connected [10] and stand-alone applications [11]. Extension to four-wire systems allows better performances with single-phase loads [12]. Recently, DFIGs have been explored as an option for on-board power generation to supply a variable-frequency power system [8].

The impact of electrical perturbations on the DFIG flux and torque has been thoroughly analysed in wind applications, focusing on the effects of faults [13], imbalance [14] and voltage distortion [15]. Mitigating strategies are based on the injection of appropriate rejection signals through advanced controllers [14]. These studies address grid-connected rather than stand-alone systems and the analysis is conducted only on the DFIG electrical system, without considering the drive-train dynamics. Also, mitigating strategies for unbalanced- or distorted-load

effects are mainly concerned with steady-state torque components pulsating at multiples of the stator frequency, typically the second and sixth harmonic. However, dynamic modulated loads in stand-alone systems produce also a different kind of torque perturbation at much lower frequency and much closer to the dominant modes of the drivetrain [16]; this is also seen in wind loading on vertical axis wind turbines [17]. Mitigation strategies blocking critical frequencies from propagating through the control chain have been proposed in some industrial drives [18], but they need appropriate knowledge on the nature of the electromechanical interactions.

The literature shows little work on electro-mechanical interactions in stand-alone systems, especially regarding DFIGs. The analysis in [19] identified drive-train dominant modes, but the excitation of resonant modes by switching loads, is supported by simulation only. Time-step simulation and numerical eigenvalue analysis appear to be the preferred tools to study electromechanical systems, but they do not give direct insight into the impact of system and control parameters on the electromechanical interactions.

The motivation for this research was to develop a systematic approach to evaluate the effect of control parameters and electrical load conditions on the excitation of mechanical resonances. This paper presents and validates a simplified electromechanical model for a stand-alone DFIG coupled to a mechanical system that can be used in many power applications from power generation to transport. The early work this paper links through had its main focus on variable-frequency power generation to supply aircraft power systems, so experimental validation is conducted on a scaled test platform which was designed specifically to represent the electromechanical system behaviour of a Rolls-Royce Trent 1000 gas turbine power off-take [19]. Nonetheless, the rig can also replicate the behaviour of other electro-mechanical systems that require a gearbox to change the relative speed to the prime mover. ~~Since the main contribution of this work is to create a model able to analyse the frequency response of an electro-mechanical system. The main contribution of this paper is the frequency domains analysis of interactions between the mechanical and the electrical elements, including the contribution of the control schemes but analysed as a complete system looking for perturbations in the mechanical or electric signals. This analysis can be expanded to other control schemes, deriving separate transfer functions for mechanical and electrical systems and then combining them to create a full electro-mechanical model for the complete system, giving the flexibility to put in place any control scheme.~~

The main contribution of this paper is the frequency domain analysis of interactions between the mechanical and the electrical subsystems, including the contribution of the control schemes and accounting for the coupling among control, electric and mechanical modes and perturbations. Being based on analytical transfer functions, this integrated analysis approach gives strong insight into the interaction mechanism between subsystems and can be easily extended to incorporate other control schemes and components in the full electromechanical model.

~~Its~~ The frequency response is ~~then~~ validated against experimental results. The frequency domain model is used to show how changes in electrical load and controller gains affect the excitation of resonant modes.

## 2. Mechanical system

The mechanical system for this analysis is composed of a DC motor and a flywheel, coupled with a set of drive shafts, gearbox, DFIG, and a smaller flywheel to represent the inertia of a second generator, as shown in Fig. 1 [20]. The system in Fig. 1 can be represented by a set of five second-order motion equations written in matrix form in (1)

$$\mathbf{M}\ddot{\mathbf{q}} + \mathbf{C}\dot{\mathbf{q}} + \mathbf{K}\mathbf{q} = \mathbf{Q} \tag{1}$$

where **q** is the vector of free angular coordinates, as shown in Fig. 1 and **Q** is the vector of forcing terms. The mass, damping and stiffness matrices **M**, **C**, and **K** are defined in the Appendix.

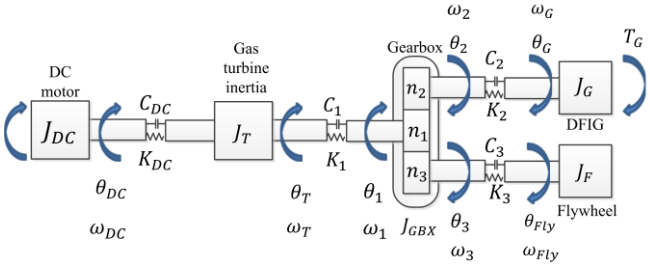


***Fig. 1.*** *Description of the mechanical platform*

$$\mathbf{q} = \begin{bmatrix} \theta_{DC} & \theta_T & \theta_G & \theta_{Fly} & \theta_1 \end{bmatrix} \tag{2}$$

$$\mathbf{Q} = \begin{bmatrix} T_{DC} & 0 & T_G & 0 & 0 \end{bmatrix}^T \tag{3}$$

The natural (undamped) frequencies are related to the **M** and **K** matrices, where there is more uncertainty in the values of the **K** matrix, since the stiffness of the driveline assembly of shafts, couplings and bearings is less well defined.

$$\omega_{nk} = \sqrt{eig(\mathbf{M}^{-1}\mathbf{K})} \tag{4}$$

Equation (4) predicts five different frequency values, including the trivial eigenvalue ωn0=0 corresponding to the rigid motion of the whole system. The four remaining modes are associated with the interaction between the DFIG, flywheel (and DC motor) and generator flywheel shafts, as well as the gearbox, and are shown in Table 1. A reduced-order model created by neglecting the DC motor and gearbox inertias eliminates the high frequency components in the frequency analysis, which are difficult to identify in the laboratory tests, and gives as a result the two low frequency components which are then the first and second resonant modes identified in [19]. The inertia of the gearbox is the lumped inertia of all the gears but referred to the dc motor side. In Table 1, the predicted natural frequencies modes for the complete model are compared with the real values obtained in [19].

**Table 1** Natural frequencies

| Natural mode | Predicted (Hz) | Tested (Hz) |
|---|---|---|
| $f_{n1}$ | 15.5 | 13.3 |
| $f_{n2}$ | 19.5 | 20.0 |
| $f_{n3}$ | 90.7 | - |
| $f_{n4}$ | 154.8 | - |

## 3. Electrical system

The electrical system is composed of a DFIG controlled equipped with current and stator voltage sensors and controlled by a Voltage Source Inverter (VSI) via a

dSPACE platform. The system parameters are given in Table 2 in the Appendix. Two rotor current controllers and a stator voltage controller are implemented in the dq axis to control the DFIG [11].

### 3.1. Complete control scheme

The complete controller scheme is shown in Fig. 2, where both voltage and current controllers are implemented in the system, using a resistive load to test the controller.

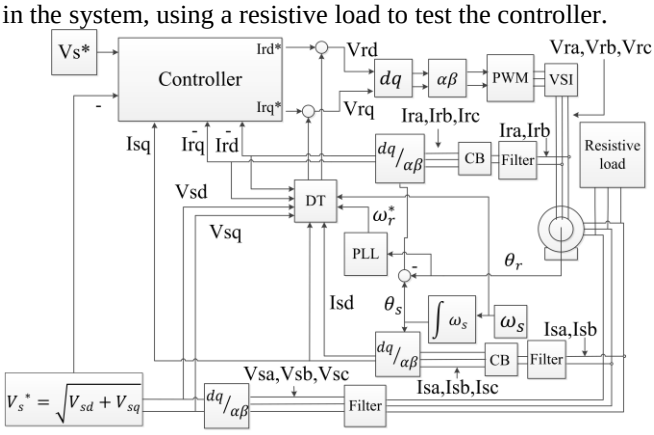


CB: Current Block, DT: Decoupling terms, PLL: Phase Locked Loop.

***Fig. 2.*** *DFIG controller scheme*

The grid-side converter (GSC) is not considered in this paper, because the main aim of this study is to provide a tool for analysing electromechanical interactions arising from mechanical excitations and load changes. In usual DFIGs, the GSC is synchronized to the stator via fast current control loops and typically operates at unity power factor. The usually large time constant of the dc-link makes the GSC and the rotor current dynamics reasonably uncoupled, resulting in the GSC behaving like a current source to regulate the minor power flow across the rotor.

### 3.2. DFIG model

Machine equations taken from [21] are used to develop the analysis, simulation and control of the DFIG. Two axis equations in a general reference frame are presented in (5) to (9) using motoring conventions, and the DFIG equivalent circuit is shown in Fig. 3: circuit parameters are referred to the stator.

$$\bar{v}_s = R_s \bar{i}_s + \frac{\mathrm{d}\,\bar{\psi}_s}{\mathrm{d}\,t} + j\,\omega_s \bar{\psi}_s \tag{5}$$

$$\bar{v}_r = R_r \bar{i}_r + \frac{\mathrm{d}\,\bar{\psi}_r}{\mathrm{d}\,t} + j\left(\omega_s - \omega_r\right)\bar{\psi}_r \tag{6}$$

$$\bar{\psi}_s = L_s \bar{i}_s + L_m \bar{i}_r \tag{7}$$

$$\bar{\psi}_r = L_m \bar{i}_s + L_r \bar{i}_r \tag{8}$$

$$T_G = -pp\,\frac{L_m}{L_s}(\bar{\psi}_s \times \bar{i}_r) \tag{9}$$

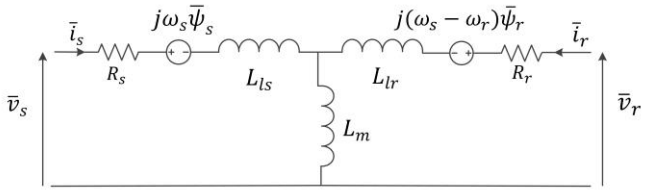


***Fig.3.*** *Equivalent circuit for the DFIG*

### 3.3. DFIG control

Two nested control loops are used, the outer for the stator voltage and the inner for the rotor currents [11]. The experimental system is designed with set-points for voltage and frequency of 400 V line-to-line and 50 Hz. The bandwidth of the current controller was originally set at 1/5 of the switching frequency, but due to the use of filtering in the platform, it was reduced to 500 Hz. The use of 15 Hz for the outer voltage controller is discussed in Section 3.5.

Stator frequency regulation is achieved using a reference angle $\theta_s^*$ for driving the stator flux:

$$\theta_s^* = \int \omega_s^* dt \tag{10}$$

Where $\omega_s^*$ is the stator reference frequency and $\theta_r = pp\theta_G$. The slip angle estimated by

$$\theta_{slip} = \theta_s^* - \theta_r \tag{11}$$

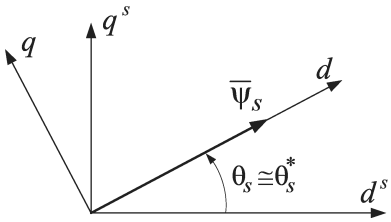


***Fig. 4.*** *Stator flux alignment in the DFIG*

and used in the reference frame transformations to calculate dq quantities as seen in Fig.4, where $\theta_r = pp\theta_G$. The orientation along the stator flux is then obtained with the open-loop control strategy in [11], setting the q-axis reference rotor current in such a way as to have zero q-axis flux according to (7)

$$i_{rq}^* = -\frac{L_s}{L_m} i_{sq} \tag{12}$$

### 3.4. Current control

A Pseudo Derivative Feed Forward (PDFF) controller scheme is chosen for the inner current loop as shown in Fig. 5 in a state space form, using the DFIG as the controller plant. This scheme has been implemented in a PMSM speed controller as seen in [22]. The PDFF controller scheme is selected for the current controller looking for flexibility to tune the closed loop zeros that have a direct effect on the rise time in the system, and at the same time tune the noise rejection in the system and the overshoot [23]. The cross-coupling terms (CTs) in Fig. 5 are assumed to be cancelled by the decoupling inputs (DTs) as detailed in (13)-(14).

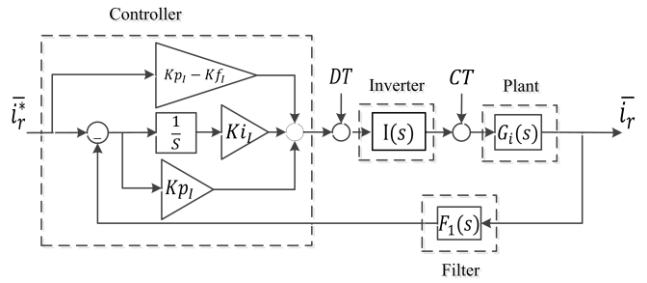


***Fig.5.*** *Current controller for the DFIG*

$$DT(v_{rd}) = -(\omega_s^* - \omega_r)\left(L_r - \frac{L_m^2}{L_s}\right) i_{rq} \quad (13)$$

$$DT(v_{rq}) = (\omega_s^* - \omega_r)\left(\frac{L_m}{L_s}\left(\frac{v_{sq} - i_{sq}R_s}{\omega_s^*}\right) + \left(L_r - \frac{L_m^2}{L_s}\right) i_{rd}\right) \quad (14)$$

In Fig. 5, the terms $Kp_i$ ,$Kf_i$ and $Ki_i$ are the controller gains and $G_i(s)$ is the rotor DFIG transfer function. The VSI is treated as ideal, apart from computation delays which are represented by $I(s)$ [24]. $F_1(s)$ represents the anti-aliasing filter. These effects are defined by (15) and (16):

$$I(s) = \frac{1}{0.5t_s s + 1} \quad (15)$$

$$F_1(s) = \frac{\omega_f}{s + \omega_f} \quad (16)$$

where the terms $t_s$ and $\omega_f$ are the switching period for the VSI (0.2 ms) and the filter cutoff frequency (720 Hz) for the sensors in the platform respectively.

$$G_i(s) = \frac{1}{R_r + \sigma L_r s} \quad , \quad \sigma = 1 - \frac{L_m^2}{L_s L_r} \quad (17)$$

### *3.5. Voltage plant model and control*

A PI controller is used for this application with a bandwidth of at least 10 times slower than the current controller. The voltage controller plant is derived accounting for variations in the stator flux and load.

Assuming perfect alignment on the stator flux, (7) gives:

$$\psi_{sd} = L_s i_{sd} + L_m i_{rd} \approx \psi_s \ , \psi_{sq} = L_s i_{sq} + L_m i_{rq} \approx 0 \quad (18a,b)$$

With small-signal perturbations, denoted with $\Delta$, (18-a) gives:

$$\Delta i_{sd} = -\frac{L_m}{L_s}\Delta i_{rd} + \frac{1}{L_s}\Delta\psi_{sd} \quad (19)$$

Neglecting the stator resistance and again assuming perfect orientation – namely neglecting any error in the stator frequency, the stator equation (5) is split into:

$$\Delta v_{sd} \approx s\Delta\psi_s \quad , \ \Delta v_{sq} \approx \Delta(\omega_s \psi_s) \approx \omega_s^* \Delta\psi_s \quad (20)$$

The voltage plant is completed including the transfer functions between d-axis stator current, flux and voltage components. By considering a purely resistive load and accounting for perturbations in the load resistance *RL*

$$\Delta v_{sd} = -(i_{sd0}\Delta R_L + R_{L0}\Delta i_{sd}) = -R_{L0}\Delta i_{sd} \quad (21)$$

because $i_{sd0}$=0. Similarly, the perturbation of the stator voltage magnitude is simply

$$\Delta v_s = \Delta\left(\sqrt{v_{sd}^2 + v_{sq}^2}\right) = \frac{v_{sd0}\Delta v_{sd} + v_{sq0}\Delta v_{sq}}{\sqrt{v_{sd0}^2 + v_{sq0}^2}} = \Delta v_{sq} \quad (22).$$

Equations (19)-(22) are summarized in the block diagram in Fig. 6, which provides the plant transfer function for the voltage controller design.

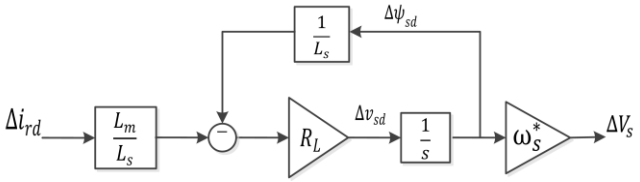


***Fig.6.*** *Voltage plant for the resistive load*

The model in Fig. 6 allows for small variations in the stator flux that will be reflected in the changes in stator voltage around an operating point. Further analysis was done looking for the stability and noise rejection of the system resulting in an optimal range of bandwidths of 13 to 20 Hz for the outer controller, so a value of 15 Hz for the voltage controller was selected. Care must be taken in designing the controller, since any possible interaction in the system could be amplified around the cut-off frequency of the controller.

## 4. Electro-mechanical system

Frequency analysis using the separate transfer functions of the different individual mechanical and electrical systems is presented in the next section, where all the individual equations are merged to form a transfer function of the complete electro-mechanical system. A simplified model of an ideal gearbox is used since the contribution of the separate elements was analysed, both mathematically and experimentally, with little contribution on the magnitude of the frequency components. The inductance ratio *Ls/Lm* in (12) is supposed exactly known and the current controller is assumed fast enough to achieve an almost instantaneous field orientation through (10)-(12). Also, the decoupling terms present in the current controller are considered in the transfer function analysis to perfectly cancel the cross-coupling terms in the DFIG equations, without affecting the main loop.

### *4.1. Electrical system transfer functions*

The transfer function analysis takes into account the individual contribution of the elements in the system. The transfer function $Fi(s)$ of the closed-loop current controller is derived from Fig. 5 and given in (23).

$$Fi(s) = \frac{\Delta i_{rd}}{\Delta i_{rd}^*} = \frac{\Delta i_{rq}}{\Delta i_{rq}^*} = \frac{G_i(s)I(s)\left[kp_I + \frac{ki_I}{s}\right]}{1 + F_1(s)G_i(s)I(s)\left[kf_I + \frac{ki_I}{s}\right]} \quad (23)$$

From (20)-(22) and Fig.6, the transfer function of the voltage plant is

$$G_v = \frac{\Delta v_s}{\Delta i_{rd}} = \frac{\omega_s^* L_m}{1 + \frac{L_s}{R_L} s} \tag{24}$$

The PI voltage controller *Cv(s)* and the closed-loop voltage control transfer function *Fv(s)* are given in (25)-(26).

$$C_v(s) = Kp_v + \frac{Ki_v}{s} \tag{25}$$

$$F_v(s) = \frac{\Delta v_{sq}}{\Delta V_s^*} = \frac{C_v(s) Fi(s) G_v(s)}{1 + C_v(s) Fi(s) G_v(s) F_2(s)} \tag{26}$$

With the assumption of purely resistive load invoked in Section 2 and accounting for variations in the load resistance *RL*, the perturbation in the stator current is

$$\Delta i_{sq} = -\frac{1}{R_{L0}} \Delta v_{sq} + \frac{V_{s0}^*}{R_{L0}^2} \Delta R_L \tag{27}$$

The perturbation in the q-axis rotor current follows from (18-b) and (27):

$$\Delta i_{rq} = -\frac{L_s}{L_m} \Delta i_{sq} = \frac{1}{R_{L0}} \frac{L_s}{L_m} \Delta v_{sq} - \frac{V_{s0}^*}{R_{L0}^2} \frac{L_s}{L_m} \Delta R_L \tag{28}$$

The linearization of the torque equation (9) under field-oriented conditions (18) gives

$$\Delta T_G = -pp \frac{L_m}{L_s} \left\{ i_{rq0} \Delta \psi_{sd} + \psi_{sd0} \Delta i_{rq} \right\}, \quad k_T = pp \frac{L_m}{L_s} \tag{29}$$

Equation (29) needs to be rewritten in terms of the inputs $\Delta V_s^*$ and $\Delta R_L$. To this purpose, $\Delta i_{rq}$ and $\Delta \psi_{sd}$ are first expressed in terms of $\Delta v_{sq}$ and $\Delta R_L$ using (28) and (20-b), and finally $\Delta v_{sq}$ is eliminated using $F_v(s)$ in (26). Since the relationship $i_{rq0} = -(L_s/L_m)\ i_{sq0} = (L_s V_{s0}^*/L_m R_{L0})$ is used, the resulting expression is:

$$\Delta T_G = -\frac{pp V_{s0}^*}{R_{L0} \omega_s^*} \left( 2F_v(s) \Delta V_s^* - \frac{V_{s0}^*}{R_{L0}^2} \Delta R_L \right) \tag{30}$$

From (30), the transfer function between reference voltage and DFIG torque follows

$$FE(s) = \frac{\Delta T_G}{\Delta V_s^*} = -\frac{2 pp V_{s0}^*}{R_{L0} \omega_s^*} F_v(s) \tag{31}$$

Fig. 7 shows the diagram of the electromechanical system. In this simplified model, there is no feedback from the mechanical system to the electrical. It has to be noted that the effects of the *irq* controller (finite dynamics) are neglected in the transfer function analysis since a perfect alignment in the stator flux is considered. Provided that the measurement of rotor angle is correct, the electrical system should not be affected by the excitation of mechanical natural modes, but the mechanical system is highly susceptible to disturbances coming from the electrical side.

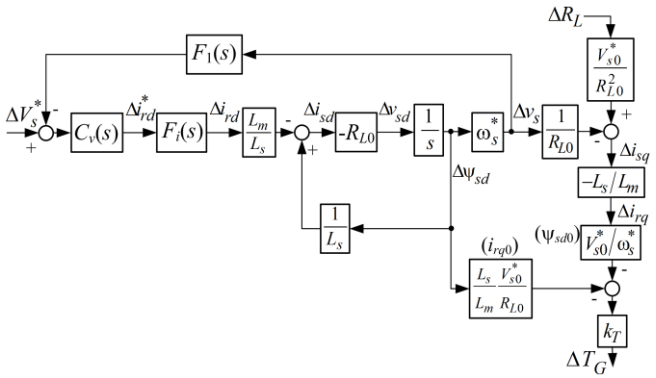


***Fig.7.*** *Block diagram of the electro-mechanical system*

### *4.2. Mechanical system transfer function*

The mechanical transfer function *FM*(s)

$$FM(s) = \frac{K_2 \Delta(\theta_2 - \theta_G)}{\Delta T_G} \tag{32}$$

linking electromagnetic torque $\Delta T_G$ and DFIG shaft torque perturbations $K_2\Delta(\theta_2 - \theta_G)$ is developed using mechanical matrix equation (1) with the matrices given in the Appendix which take into account the full system. Algebraic manipulations have been carried out with Wolfram-Mathematica leading with a very complicated structure which is not reported in this paper. However, a reduced-order mechanical model can also be implemented in the analysis since the frequency components associated with the gearbox and the DC machine inertia can be neglected.

### *4.3. Complete system transfer function*

The relevant inputs for the electrical system are voltage and load perturbations $\Delta V_s^*$ and $\Delta R_L$. They are linked to the DFIG shaft torque perturbation by combining (32) with (31) and (30)

$$FEM_V(s) = K_2 \frac{\Delta(\theta_2 - \theta_G)}{\Delta V_s^*} = FE(s) FM(s) \tag{33}$$

$$FEM_R(s) = K_2 \frac{\Delta(\theta_2 - \theta_G)}{\Delta R_l} = \frac{pp V_s^{*2}}{\omega_s^* R_{L0}^3} FM(s) \tag{34}$$

The frequency response from (34) is presented in Fig. 10 a) using a value of 12 Ω as the base value for the electric load, which represents the full load value of the DFIG. The mechanical resonances can be identified in response to changes in reference voltage and electrical load.

## 5. Transfer function validation

Fig. 8 a) represents the frequency response of the system and compares the values from (31) with experimental results obtained by introducing a sinusoidal disturbance on the voltage controller reference value. The analysis is compared and validated with laboratory results, circular dots (o) and time domain simulation, cross markers (x). The simulation has been validated against the model presented in [19].

The electrical transfer function in Fig. 8 a) shows little attenuation to disturbance at low frequencies, with a

first order roll-off due to the voltage controller with a corner frequency of 15 Hz, and a higher-order roll-off at 500 Hz due to the current controller. Hence disturbances in voltage can excite the mechanical natural modes, with a gain of 1-10NmV$^{-1}$. The sensitivity changes linearly with load current. The current controller gains have little effect on how disturbances on voltage are passed through to the mechanical system. However, in cascade control, the bandwidth of the inner current loop does set limits on the bandwidth of the outer voltage loop. Differences in phase angles can also be noted in Fig. 8 b), where the simulation results seem to have a tendency to increase this angle at higher frequency. Overall, the results confirm the small signal analysis, especially for the magnitude of the frequency response.

Fig. 8 c) shows the frequency response of the electro-mechanical system, with three values of resistive load considered for small variations on the reference voltage. Mechanical resonances appears also in $FEM_V(s)$

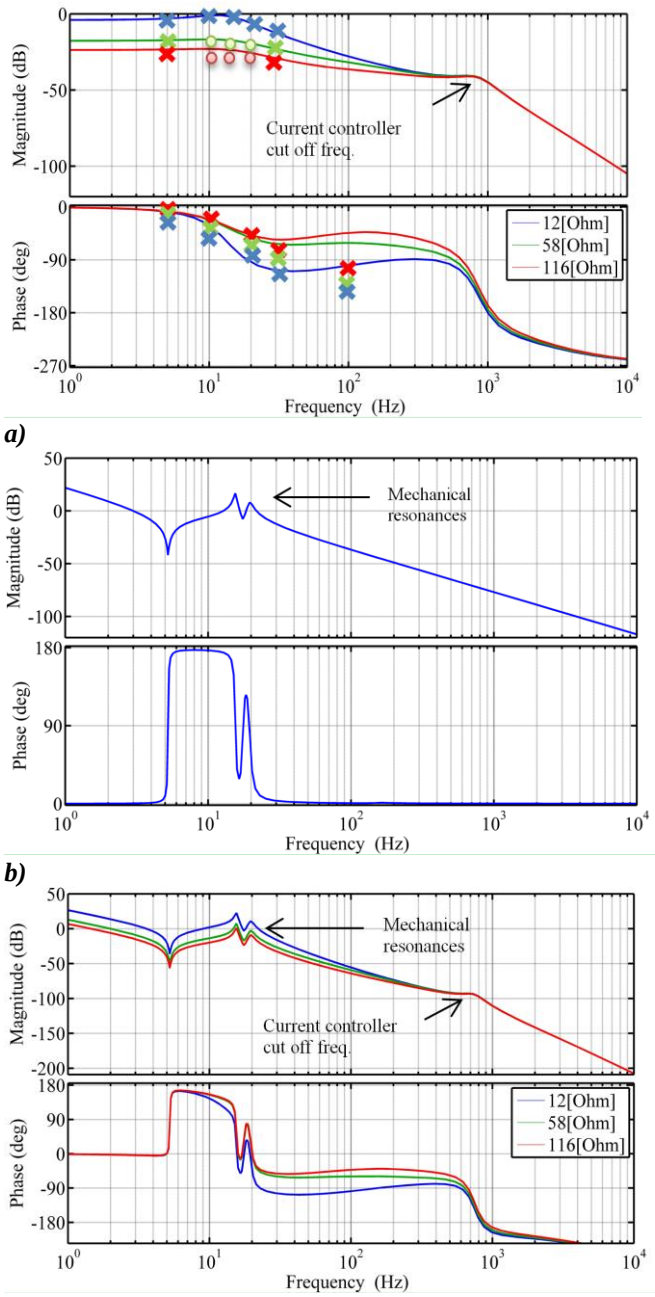


***Fig.8.*** *Frequency response of the different transfer functions:* ***a)*** *FE (s) (31),* ***b)*** *$FEM_R$ (s) (34),* ***c)*** *$FEM_V$(s) (33)*

## 6. Laboratory results

The electro-mechanical platform described in [20] and Fig.1 is used to analyze the interactions in the system. The rotor side is supplied by a 700 Vdc voltage source inverter implemented with a braking resistor for the super synchronous regime. Only torque reading from the DFIG shaft is available in the results. A brake was applied to the fly-wheel generator inertia looking to eliminate possible variations in the stiffness due to backlash. Results are presented for three different rotor speeds ($\omega_r$). 800 rpm, 1000 rpm and 1200 rpm (*slip*=0.2, 0 and -0.2). All the tests are in steady-state for two load values of 116 Ω and 58 Ω per phase, corresponding to a stator load of 0.2 p.u to 0.4 p.u.

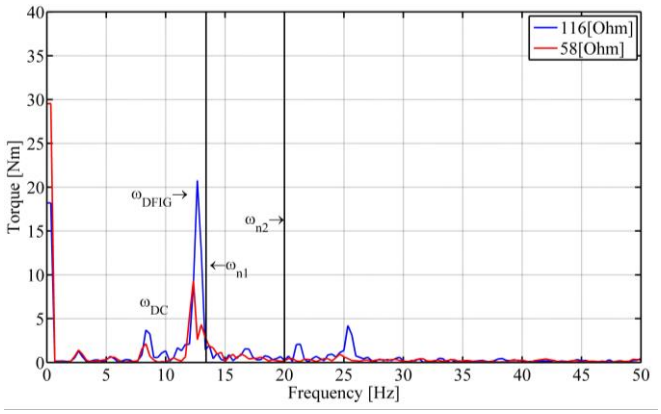


*a)*

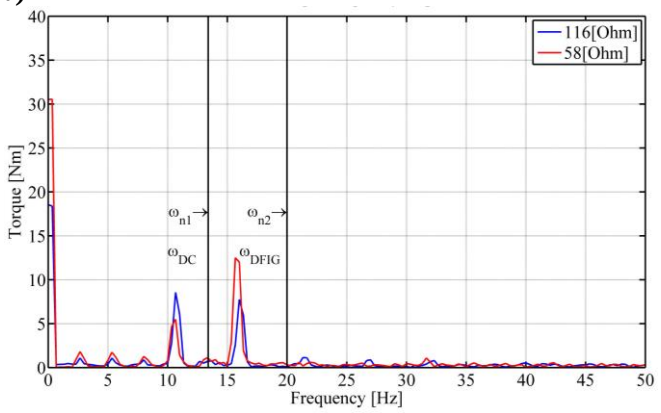


*b)*

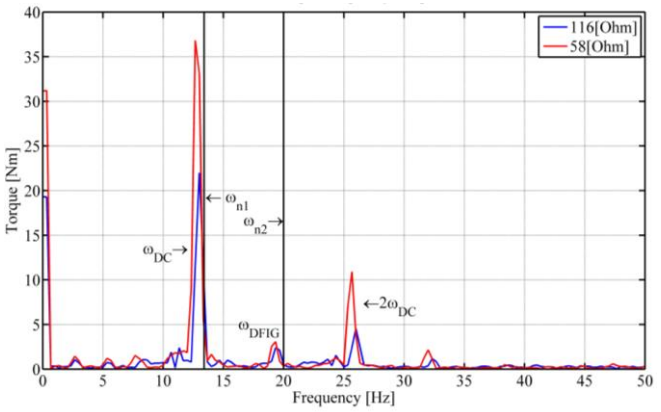


*c)*

***Fig.9.*** *DFIG shaft torque frequency response* ***a)*** *ωr=800 rpm,* ***b)****1000 rpm,* ***c)****1200 rpm*

From Fig. 9 it is possible to identify the impact of the speed of both the DC machine and the DFIG ($\omega_{DC}$ and $\omega_{DFIG}$ respectively) on the torque response in the system, which is attributed to mechanical unbalance. Fig 9 also shows a frequency component at 2ωDC. Two resonant modes are present in the DFIG torque analysis, the first one appearing at around 13 Hz and the second at 22 Hz, identified by the dashed lines. If this mechanical excitation is close to a natural mode, then the torque component is amplified, as shown in Figs. 9 a) and c). No frequency components associated with the gearbox or DC inertias were identified.

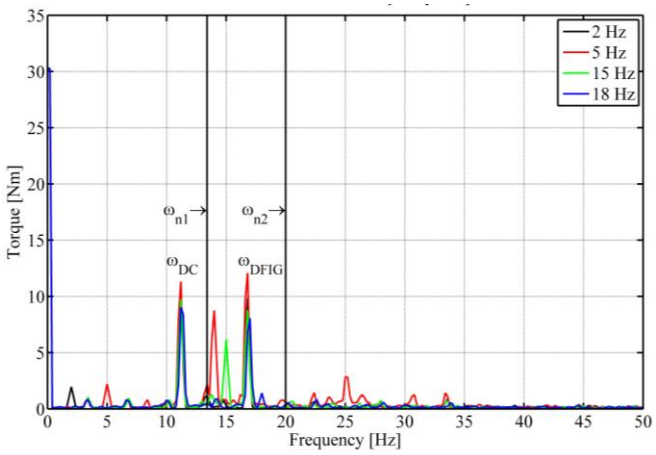


*a)*

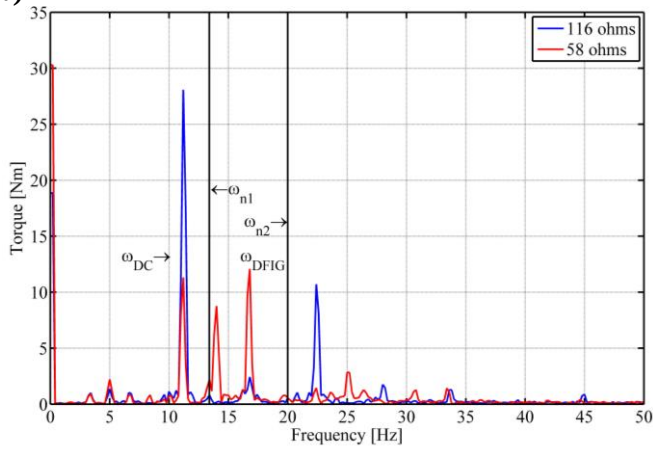


*b)*

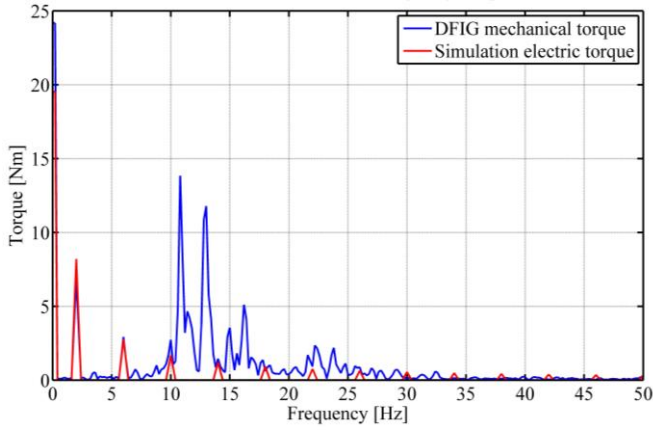


*c)*

***Fig.10.*** *DFIG shaft torque frequency response* ***a)*** *Rl=58 ohms with different frequency injection,* ***b)*** *disturbance only at 5Hz,* ***c)*** *using a switching load at 2 Hz*

Figs. 10 a) and b) show the effect on the DFIG shaft torque when a 15V disturbance is injected into the reference voltage for the frequencies and loads shown at 1000rpm shaft speed.

This method was used to obtain the results in Fig 8 c) to validate the small signal analysis and confirm that disturbances in the electrical system couple through to the mechanical system.

Fig 10 c) shows the frequency response of the measured mechanical torque in the DFIG shaft and the estimated electric torque on the DFIG at 1000 rpm. This

experiment was performed by switching a resistive load with a frequency of 2 Hz between two resistive values of 0.2pu and 0.4pu with a duty cycle of 50%. The torque analysis shows that the odd harmonics are present in the system as a result of the load switching. Results using 1Hz and 3Hz were also evaluated but the 2Hz switching shows a stronger impact since the 7th harmonic is closer to the predicted 1st resonant mode.

Fig. 10 a) shows that electrical oscillations can be introduced into the mechanical system by a perturbation coming directly from the voltage reference. From Fig. 8 c) the current controller has a sharp cut-off, which significantly attenuates torque but only above the cut-off frequency of 500 Hz. It sets an upper limit on the voltage bandwidth and also allows ideal orientation to be assumed over the range of mechanical frequencies of interest. In contrast, the voltage bandwidth could be reduced to introduce attenuation of the 13 Hz and 22 Hz frequency components. However, the benefit in terms of additional attenuation is small as the roll-off is gentle, there would be an impact on the voltage regulation, and the voltage loop becomes unstable for a bandwidth below 13 Hz if the same damping factor is set in the tuning of the system. There is a linear relationship between load current and magnitude of the torque disturbance, Fig. 10 b) shows that the excitation of resonant modes is greater at higher loads. Changes in load can therefore excite the resonant modes, particularly if the load is switched at the resonant frequency or a subharmonic thereof.

Asymmetries present in the system (for example electrical unbalance or bearing wear) introduce additional disturbances in the torque, speed and current of the DFIG [25]. The frequency and magnitude of the disturbance depend on the nature of the asymmetry and the point of operation, and can also be related to low frequency components in the rotor. As Fig. 10 c) shows, a change in load level gives significant changes in which frequency components are present.

## 7. Conclusion

The main contribution of this work is the development of a frequency domain model for analysing the electromechanical interactions in a DFIG-based generator system. The proposed model identifies critical resonances in the system that can be triggered by both mechanical and electrical excitations in the platform. In this paper a transfer function analysis uses the whole system to show that disturbances in the electrical load couple directly into the mechanical system with little or no attenuation at the frequencies of the natural resonant modes. However, the mechanical disturbances do not feed back into the electrical system, provided that the orientation and decoupling are correct. Theoretical and experimental results show that low-frequency switched electrical loads can excite the resonant modes in the system through the harmonics induced in the torque.

The experimental work has shown that torque pulsations are also introduced into the mechanical system by mechanical unbalance at multiples of the rotor speeds. The ratio of 1.5, between the DFIG and DC motor speeds, set by the gearbox, can be seen in the frequency response of the DFIG shaft. It also can be seen that these perturbations are proportional to the torque required from the electric generator as seen in figure 9 and 10, meaning that these effects will be more evident at higher power levels (lower resistance), especially at rated torque and overload situations.

Voltage loop tuning parameters appear to be crucial for the attenuation or amplification of the resonant frequencies. Torque disturbances can be attenuated by the correct tuning in combination with the use of filters as seen in [18]. The transfer function analysis is a powerful tool and can be used to investigate control-based solutions to block those harmful frequencies that can excite resonant modes on the mechanical drivetrain. Although the analysis has been developed for a DFIG, the approach is general and could be applied to other generator technologies and drivetrain configurations.

## 8. Acknowledgments

The authors would like to thank … To be added after the review process

## 9. References

[1] J. C. Wachel, "Analysis of Torsional Vibrations in Rotating Machinery," in *Procedings of the Twenty-Second Turbomachinery Symposium*, 1993.

[2] L. Ran, D. Xiang, and J. L. Kirtley, "Analysis of Electromechanical Interactions in a Flywheel System With a Doubly Fed Induction Machine," *IEEE Transactions on Industry Applications*, vol. 47, pp. 1498-1506, 2011.

[3] P. Wheeler and S. Bozhko, "The More Electric Aircraft: Technology and challenges," IEEE Electrif. Mag., vol. 2, pp. 6-12, 2014.

[4] B. Sarlioglu and C. T. Morris, "More Electric Aircraft: Review, Challenges, and Opportunities for Commercial Transport Aircraft," *IEEE Trans. Transport. Electrif.*, vol. 1, pp. 54-64, 2015.

[5] F. Mei and B. Pal, "Modal Analysis of Grid-Connected Doubly Fed Induction Generators," *IEEE Trans. En. Conv.*, vol. 22, pp. 728-736, 2007.

[6] L. A. Lopes, J. Lhuilier, M. F. Khokar, and A. Mukherjee, "A Wind Turbine Emulator that Represents the Dynamics of the Wind Turbine Rotor and Drive Train," *in 2005 IEEE 36th Power Electronics Specialists Conf.*, 2005, pp. 2092-2097.

[7] M. Singh, E. Muljadi, and J. Jonkman, "Hybrid Electro-mechanical Simulation Tool for Wind Turbine Generators," *in 2013 IEEE Green Techn. Conf.*, 2013, pp. 266-270.

[8] T. Feehally and J. M. Apsley, "The Doubly Fed Induction Machine as an Aero Generator," *IEEE Trans. Ind. Appl.*, vol. 51, pp. 3462-3471, 2015.

[9] R. Cardenas, R. Pena, S. Alepuz, and G. Asher, "Overview of Control Systems for the Operation of DFIGs in Wind Energy Applications," *IEEE Trans. Ind. Electron.*, vol. 60, pp. 2776-2798, 2013.

[10] R. Pena, J. C. Clare, and G. M. Asher, "Doubly fed induction generator using back-to-back PWM converters and its application to variable-speed wind-energy generation," *IEE Proc. Electr. Pow. Appl.* , vol. 143, pp. 231-241, 1996.

[11] R. Pena, J. C. Clare, and G. M. Asher, "A doubly fed induction generator using back-to-back PWM converters supplying an isolated load from a variable speed wind turbine," *IEE Proc. Electr. Pow. Appl.*.vol. 143, pp. 380-387, 1996.

[12] G. Carrasco, C. A. Silva, R. Peña, and R. Cárdenas, "Control of a Four-Leg Converter for the Operation of a DFIG Feeding Stand-Alone Unbalanced Loads," *IEEE Trans. Ind. Electron.*, vol. 62, pp. 4630-4640, 2015.

[13] H. Geng, C. Liu, G. Yang, "LVRT Capability of DFIG-Based WECS Under Asymmetrical Grid Fault Condition," *IEEE Trans. Ind. Electron.*, vol. 60, no. 6, pp. 2495-2509, June 2013.

[14] H. Nian, T. Wang and Z. Q. Zhu, "Voltage imbalance compensation for doubly fed induction generator using direct resonant feedback regulator," in *IEEE Trans. Energy Convers.*, vol. 31, no. 2, pp. 614-626, June 2016.

[15] H. Xu, J. Hu, and Y. He, "Operation of wind-turbine-driven DFIG systems under distorted grid voltage conditions: Analysis and

experimental validations," *IEEE Trans. Power Electron.*, vol. 27, no. 5, pp. 2354–2366,May 2012..
[16] C. Ahumada, S. Garvey, T. Yang, P. Wheeler, and H. Morvan, "The Importance of Load Pulse Timing in Aircraft Generation," *in 18th Intl. Conf. on Elec. Machines and Systems*, Pattaya city, Thailand, 2015.
[17] D. J. Breslan, J. M. Apsley, A. C. Smith, S. G. Kirkham, and K. J. Towell, "Control of a vertical axis wind turbine in gusty conditions," in *8th IET International Conference on Power Electronics, Machines and Drives (PEMD 2016)*, 2016, pp. 1-6.
[18] M. A. Valenzuela, J. M. Bentley, A. Villablanca, and R. D. Lorenz, "Dynamic compensation of torsional oscillation in paper machine sections," *IEEE Trans. Ind. Appl.*, vol. 41, pp. 1458-1466, 2005.
[19] T. Feehally, I. Erazo-Damián, and J. M. Apsley, "Analysis of Electromechanical Interaction in Aircraft Generator Systems," *IEEE Trans. Ind. Appl.*, vol. 52, pp. 4327-4336, 2016.
[20] T. Feehally, "electro-mechanical interaction in gas turbine-generator systems for more-electric aircraft," PhD thesis, School of Electrical and Electronic Engineering, University of Manchester, Manchester, 2012
[21] P. C. Krause, Analysis of electric machinery: McGraw-Hill, 1986.
[22] S. Cheng, Y.-Y. Huang, H.-H. Chou, C.-M. Ting, C.-M. Chang, and Y.-M. Chen, "PDFF and H∞ Controller Design for PMSM Drive," in Nov. Algorithms and Tech. In Telecom., Autom. and Indust. Electron, T. Sobh, K. Elleithy, A. Mahmood, and M. A. Karim, Eds., ed Dordrecht: Springer Netherlands, 2008, pp. 237-241
[23] D. Y. Ohm, "Analysis of PID and PDF compensators for motion control systems," *in IEEE Ind. Appl. Soc. An. Meet* , 1994, pp. 1923-1929 vol.3.
[24] B. Zigmund, A. A. Terlizzi, X. d. T. Garcia, R. Pavlanin, and L. Salvatore, "Experimental Evaluation of PI Tuning Techniques for Field Oriented Control of Permanent Magnet Synchronous Motors," *Advances in Electrical and Electronic Engineering*, vol. 5, pp. 114-119, 2011.
[25] S. Djurovic and S. Williamson, "Losses and pulsating torques in DFIGs with unbalanced stator and rotor excitation," *in 2008 IEEE International Conference on Sustainable Energy Technologies*, 2008, pp. 328-333.

## 10. Appendices

**Table 2** Drive Train and DFIG Parameters

| | |
|---|---|
| DC Machine inertia $J_{DC}$ (kg·m$^2$) | 0.197 |
| GT flywheel inertia $J_T$ (kg·m$^2$) | 7 |
| Gearbox referred inertia $J_{GBX}$ (kg·m$^2$) | 0.052 |
| Flywheel and DFIG inertia $J_F$, $J_G$ (kg·m$^2$) | 0.359 |
| Damping standard value $C_{DC}$, $C_1$, $C_2$, $C_3$ (Nms/rad) | 3.26 |
| Turbine shaft stiffness $K_1$ (Nm/rad) | 25947.12 |
| DFIG shaft stiffness $K_2$ (Nm/rad) | 5409.58 |
| Flywheel shaft stiffness $K_3$ (Nm/rad) | 5442.38 |
| DC motor shaft stiffness $K_{DC}$ (Nm/rad) | 63240.6 |
| Gear ratios n12= n13 | 1.5 |
| Stator leakage inductance $L_{ls}$ (mH) | 3.6 |
| Stator resistance $R_s$ (Ω) | 0.2974 |
| Rotor leakage inductance $L_{lr}$ (mH) | 4 |
| Rotor resistance $R_r$ (Ω) | 0.4493 |
| Mutual inductance $L_m$ (mH) | 67.1 |

Matrices **M**, **C** and **K** in (1) are:

$$\mathbf{M} = \mathrm{diag}\left(J_{DC}, J_T, J_G, J_{Fly}, J_{GBX}\right) \tag{36}$$

$$\mathbf{C} = \begin{bmatrix} C_{DC} & -C_{DC} & 0 & 0 & 0 \\ -C_{DC} & C_{DC}+C_1 & 0 & 0 & -C_1 \\ 0 & 0 & C_2 & 0 & -n_{12}C_2 \\ 0 & 0 & 0 & C_3 & -n_{13}C_3 \\ 0 & -C_1 & -n_{12}C_2 & -n_{13}C_3 & C_1+n_{12}{}^2C_2+n_{13}{}^2C_3 \end{bmatrix} \tag{37}$$

$$\mathbf{K} = \begin{bmatrix} K_{DC} & -K_{DC} & 0 & 0 & 0 \\ -K_{DC} & K_{DC}+K_1 & 0 & 0 & -K_1 \\ 0 & 0 & K_2 & 0 & -n_{12}K_2 \\ 0 & 0 & 0 & K_3 & -n_{13}K_3 \\ 0 & -K_1 & -n_{12}K_2 & -n_{13}K_3 & K_1+n_{12}{}^2K_2+n_{13}{}^2K_3 \end{bmatrix} \tag{38}$$

where *n* refers to the gear ratio according to Table 2. In each matrix, the subscript is related to the elements displayed in Fig. 1.